

## The Optical, Electrical and Dielectric Traits of Teo<sub>2</sub>-Li<sub>2</sub>O-Licl-Eu<sub>2</sub>O<sub>3</sub> Glasses

Zahra Ashur Said Mahraz<sup>1,2\*</sup>, Siti Aishah Jupri<sup>1</sup>, ES Sazali<sup>1</sup>, MR Sahar<sup>1</sup>, KA Samah<sup>1</sup>

<sup>1</sup>Advanced Optical Materials Research Group, Department of Physics, Faculty of Science, Universiti Teknologi Malaysia, Skudai 81310, Johor, Malaysia.

<sup>2</sup>Department of Physics, College of Education-Zulten, University of Sabratha, Libya

\*Corresponding Author: Zahra Ashur Said Mahraz, Advanced Optical Materials Research Group, Department of Physics, Faculty of Science, Universiti Teknologi Malaysia, Skudai 81310, Johor, Malaysia, Tel: +6075534024, Fax: +6075566162, E-mail: mabutm.mabutm@yahoo.com

**Citation:** Zahra Ashur Said Mahraz, Siti Aishah Jupri, ES Sazali, MR Sahar, KA Samah (2021) The Optical, Electrical and Dielectric Traits of Teo<sub>2</sub>-Li<sub>2</sub>O-Licl-Eu<sub>2</sub>O<sub>3</sub> Glasses. Int J Nucl Mater 1: 1-19

**Copyright:** © 2022 Zahra Ashur Said Mahraz. This is an open-access article distributed under the terms of Creative Commons Attribution License, which permits unrestricted use, distribution, and reproduction in any medium, provided the original author and source are credited.

### Abstract

Europium oxide (Eu<sub>2</sub>O<sub>3</sub>) doped lithium tellurite glasses were prepared via melt quenching method. The effects of Eu<sub>2</sub>O<sub>3</sub> doping at varying concentration on the physical, electrical and optical properties of tellurite glasses were determined. The physical properties by means of density and molar volume are determined. Electrical and dielectric constant in the 0.01 – 10 MHz frequency range were monitored as a function of temperature (298 – 398 K). At room temperature, the conductivity and activation energy increase with increase Eu<sub>2</sub>O<sub>3</sub> concentration. Small polarons hopping (SPH) is used to explain the conduction mechanism. The density of localized state is found to decrease with increasing Eu<sub>2</sub>O<sub>3</sub> concentration in the range of  $21.3 \times 10^{20}$  to  $17.3 \times 10^{20}$  eV<sup>-1</sup> cm<sup>-3</sup>. Dielectric parameters which are dielectric constant and loss tangent are found to increase with the increase in the concentration of Eu<sub>2</sub>O<sub>3</sub>. In order to study the spectroscopic properties of fabricated glasses, absorption and emission spectroscopy has been performed. UV-Vis-NIR absorption spectra of glass samples divulged two significant peaks. Under the excitation of 393 nm laser diode, six emission bands were observed in the Eu<sup>3+</sup> single doped glasses. Increasing intensity ratio ranging from 1.13 to 2.13 with increased Eu<sub>2</sub>O<sub>3</sub> concentration is attributed to the low symmetry environment around Eu<sup>3+</sup> ions. The proposed glass system is demonstrated to be beneficial for diverse applications.

**Keywords:** Glass; Conductivity; Density of states, Dielectric properties; Optical properties

## Introduction

Nowadays, use of oxide glass materials has evolved from the simple conventional passive functions to more sophisticated active functions in many optical, electronic, structural, chemical and biochemical interdisciplinary applications [1]. Among the oxide glasses, tellurium dioxide ( $\text{TeO}_2$ )-based glasses have been widely studied because of their potential applications as compared to other conventional glasses. This is due to their high indices of refraction, large infrared transparency, high density, low melting point, high dielectric constant and electrical conductivity and good chemical durability as well as low glass transition temperature [1, 2]. Conversely,  $\text{TeO}_2$  is a conditional glass former and it cannot easily transform into the glassy state under conventional quenching conditions. Few modifiers or glass forming agents such as alkali oxides ( $\text{M}_2\text{O}$ ) are required to enhanced the glass formation ability (GFA) by breaking the Te-O-Te bridging and forms the Te-O-M bonds [3]. Tanaka *et al.* [4] study the structural of  $\text{LiCl-Li}_2\text{O-TeO}_2$  glasses and they show that, the presence of  $\text{LiCl}$  and  $\text{Li}_2\text{O}$  creates non-bridging oxygen (NBO).  $\text{Cl}^-$  and  $\text{O}^{2-}$  is considered to be fully ionized hence creates  $\text{Te-Cl}_{\text{eq}}$  bond and  $\text{Te-O}_{\text{eq}}$  bond. Since  $\text{O}^{2-}$  has a higher negative charge than  $\text{Cl}^-$ ,  $\text{O}^{2-}$  ion would donate more electrons to Te through  $\text{Te-O}_{\text{eq}}$  bond than  $\text{Cl}^-$  ion does through the  $\text{Te-Cl}_{\text{eq}}$  bond. The formation of this bond strengthened the  $\text{Te-O}_{\text{ax}}$  bond therefore the formation of  $\text{TeO}_3$  trigonal pyramid is suppressed. Iwadata *et al.* [5] states that the  $\text{TeO}_4$  trigonal bipyramids are changed into polyhedra containing NBO by the increase of  $\text{Li}_2\text{O}$  and  $\text{LiCl}$ , and then shifted to  $\text{TeO}_3$  trigonal pyramids which is considered to restrict the glass formation. This can be explained by the weakening  $\text{Te-O}_{\text{ax}}$  bond with the increase of  $\text{LiCl}$  which act as a network modifier.  $\text{LiCl}$  breaks down the  $\text{TeO}_4$  network structure by creating NBO.

Introduction of alkali ions in tellurite glasses is considered to be predominant factor playing the role of enhancing the conductivity of the glass system and hence can be applied as solid electrolytes in high density batteries, electrochromic display, fuel cell and sensors [6-8]. Tellurite based glasses exhibit relatively high dielectric constants and electrical conductivity as compared to the other glass systems, owing to the unshared pair of electrons of the  $\text{TeO}_4$  group that do not take part in the bonding [9]. The dielectric properties of tellurite glasses depend on the size of the modifier ions in the glass structure, their field strengths and the composition of the glass. The introduction of lithium is anticipated to enhance the conductivity of tellurite glass as  $\text{Li}^+$  ions are ionic conductor [10, 11]. This is because lithium is light and highly electro-positive. Consequently, lithium-based glasses find potential applications in high energy density solid state batteries [12]. Hence, the connection between the position of lithium ions in tellurite glass network and the electrical properties of these glasses is quite interesting.

Incorporation of rare earth (RE) ions such as La, Ce, Nd, Eu, Er, etc., into glasses enhances their optical properties such as refractive index, optical band gap, laser amplification and optical amplification [10, 13-15]. Recently, up-conversion (UC) luminescence of  $\text{Eu}^{3+}$  has been studied due to its favorable green and red emissions. However, it is interesting to study the electrical conductivity in these glasses to understand conduction mechanisms operated in these systems. Influence of RE ions additives on electrical conductivity of different glasses has been previously studied [10, 13-16], which indicated that the electrical conductivity depended on the glass composition and atomic size of RE ions [13]. In addition, a decrease in conductivity with the increase in the atomic weight of RE ions has been observed in different rare earth ions doped tellurite glasses, which was attributed to the low mobility of RE ions due to their heavy masses [14]. Meanwhile, tellurite glasses of composition  $80\text{TeO}_2-20\text{ZnO}$  doped with holmium ( $\text{Ho}^{3+}$ ) ions exhibited a decrease in the conductivity with the increase in holmium ionic content [15]. This was attributed to the formation of quasi-molecular complex of RE ions with the glass network. The dc and ac electrical conductivities of barium tellurite borate glass doped with  $\text{Nd}_2\text{O}_3$  having composition of  $50\text{B}_2\text{O}_3-(20-x)\text{BaO}-20\text{TeO}_2-10\text{LiF}$  or  $\text{Li}_2\text{O}$ , where  $x = 0.5, 1, 1.5$  and  $2$  mol% were measured [10]. The dc and ac conductivity values were increased, whereas the activation energy of conductivities was decreased with increasing  $\text{Nd}_2\text{O}_3$  content in the glasses containing  $\text{LiF}$ . Whereas, the addition of  $\text{Nd}_2\text{O}_3$  to glasses containing  $\text{Li}_2\text{O}$  led to decrease the conductivity and increased the activation energy [10].

Amongst of RE ions,  $\text{Eu}^{3+}$  -doped glasses find a number of applications in a variety of optoelectronic devices such as red emitting phosphors and optical storage devices [16]. By suitable selection of glass constituents, one can develop an entire range of electrical conductors, from purely ionic to purely electronic. Glasses with such properties have found applications in the development of integrated microbatteries [17]. Despite the technological and scientific relevance of tellurite glasses, the ac conductivity studies in  $\text{Eu}_2\text{O}_3$  doped lithium-tellurite glasses are far from being clarified. In this fortitude, the objective of the present work is to evaluate the physical, electrical and optical properties of the representative  $\text{TeO}_2\text{-Li}_2\text{O-LiCl}$  (TLL) glass doped with different concentration of  $\text{Eu}^{3+}$

ions. The electrical and dielectric properties of such glass samples as a function of frequency (100 Hz–1 MHz) and the temperature (298K–398K) was analyzed by employing impedance spectroscopy at 373 K.

## Experimental details

Analytical grade raw materials to prepare the  $\text{TeO}_2\text{-Li}_2\text{O-LiCl-Eu}_2\text{O}_3$  glass samples were obtained in the powder form. Pure oxides of  $\text{TeO}_2$  (Sigma-Aldrich  $\geq 99\%$ ),  $\text{Li}_2\text{CO}_3$  (Sigma Aldrich, 99.99% purity),  $\text{LiCl}$  (Fluka, 99% purity) and  $\text{Eu}_2\text{O}_3$  (Sigma Aldrich, 99.99% purity) were used as glass constituents. The prepared samples had nominal composition of  $(75-x)\text{TeO}_2\text{-}5\text{Li}_2\text{O-}20\text{LiCl-}x\text{Eu}_2\text{O}_3$  where  $x = 0.0, 0.5, 1.0, 1.5$  and  $2.0$  mol%. The raw materials with required proportion are weighted using a very sensitive weighing machine (Electronic Balance Precisa 205A SCS). The total weight of each batch of glass was 15 gram and calculated in mol%. The selected composition was placed in an alumina crucible and melted by raising the temperature of an electrical furnace (Model: Carbolite Aston Lane, Hope Sheffield S30 2RR, England) to  $900^\circ\text{C}$  for 20 minutes to achieve homogenous melting. In order to obtain transparent viscous melt, the batches were stirred frequently. The quenching process started by pouring the melt between two preheated stainless steel moulds in an alternate furnace as fast as possible to avoid solidification due to humidity. Then, the glass samples were kept at  $300^\circ\text{C}$  for about 2 hr for annealing process to reduce the thermal and mechanical strains. After two hours, the furnace was switched off and the samples were allowed to cool down gradually to room temperature ( $25^\circ\text{C}$ ). Cooling rate was a vital factor in determining the glass formation. The glass sample is cut in the dimension of  $1\text{ cm} \times 1\text{ cm} \times 1\text{ cm}$  using diamond cutter. Finally, samples are polished by diamond compound with grade point of  $1\ \mu, 3\ \mu$  and  $6\ \mu$  until each of the sample have uniform thickness  $\sim 0.2\text{ cm}$ .

The glass density ( $\rho$  in  $\text{g.cm}^{-3}$ ) is determined using Archimedes method with distilled water as an immersion liquid. Density is calculated from,

$$\rho = \frac{A_a}{A_a - B_w} \times (\rho_0 - \rho_a) \quad (1)$$

Where  $A_a$  and  $B_w$  are the weight of the sample in the air and in distilled water, respectively with  $\rho_0$  is the density of pure water and  $\rho_a$  is that of air. The molar volume ( $V_m$ ) in terms of the molecular weight ( $M$ ) yields,

$$V_m = \frac{M}{\rho} \quad (2)$$

The concentration of rare earth ion,  $N_{RE}$  is given by,

$$N_{RE} = \frac{\text{mol\%} \cdot \rho \times N_A}{V_m} \quad (3)$$

where  $\rho$  is density of the glass and  $N_A$  is the Avogadro's number. The polaron can be treated as an electron with virtual phonon. The cloud of virtual phonons resembles physically to the electron where it pulls nearby positive ions and push nearby negative ions away. Assuming the distribution of  $\text{Eu}_2\text{O}_3$  in lithium tellurite is uniform, the polaron radius  $R_p$  can be calculated by the following equation respectively,

$$R_p (\text{\AA}) = \left( \frac{1}{2} \right) \left( \frac{\pi}{6N_R} \right)^{\frac{1}{3}} \quad (4)$$

On the other hand, the inter-nuclear distance,  $R_i$  which denoted the distance between two nuclei in a molecule is calculated as following,

$$R_i (\text{\AA}) = \left( \frac{1}{N_R} \right)^{\frac{1}{3}} \quad (5)$$

The amorphous nature of glasses were examined via a Bruker D8 Advance X-ray diffractometer (XRD) which uses CuK $\alpha$  radiations ( $k = 1.54 \text{ \AA}$ ) at 40 kV and 100 mA with  $2\theta$  ranges from  $10^\circ$  to  $80^\circ$  with step size  $0.02^\circ$  and resolution of  $0.01^\circ$ . Shimadzu ultraviolet visible near infrared (UV-Vis-IR) spectrophotometer (Model: UV-1301PC) was used to record the absorption spectra of the glass samples with a resolution of 1 nm. The absorption spectrum was measured in spectral range of 200-2000 nm by using Tungsten Halogen lamp (HL) as a radiation source. Both sides of the glass samples were polished to avoid any unfavorable surface scattering during optical measurements. Perkin-Elmer photoluminescence (PL) spectra (Model: LS 55) (fitted with a pulsed Xenon lamp operates as a source of excitation) was used to measure the emission spectrum of the glass samples in visible ( $\sim 400$  to  $700$  nm) and the near infrared region (up to  $800$  nm). Gold electrodes are deposited on both side of polished glass sample using thermal evaporation technique. The conductivity measurement is done using Solartron SI 1260 Impedance/Gain-Phase Analyzer. The measurement is taken in the frequency range of 100 Hz to 1 MHz and in the temperature range of 298 K to 398 K and the voltage is kept constant at 1V. To avoid initial polarization, the measurements are started 5 minutes after voltage across samples is constant. Measurements are repeated several times to ensure the reproducibility of the data.

## Results and Discussion

### Physical properties

Table 1 summarizes the calculated physical properties of all glass samples. Compositional behavior of density and molar volume is shown in Figure 1. The decrease in glass density from  $4.88$  to  $4.73 \text{ g.cm}^{-3}$  due to the introduction of  $\text{Eu}_2\text{O}_3$ , which is ascribed to the alteration in the network structure via the generation of more NBOs. However, the density of the glass increases from  $4.73$  to  $4.77 \text{ g.cm}^{-3}$  with further addition of  $\text{Eu}_2\text{O}_3$ , which is due to higher charge and coordination number of  $\text{Eu}^{3+}$  which tend to develop highly packed glass structure [18]. The variation of molar volume with concentration of  $\text{Eu}_2\text{O}_3$  is presented in Figure 1. It is quite clear from Figure 1 that there is an increase in the molar volume from  $26.4$  to  $27.8 \text{ cm}^3.\text{mol}^{-1}$  as the concentration of  $\text{Eu}_2\text{O}_3$  is increased into the system. The molar volume is inversely proportional to density which they are expected to show opposite behavior to each other. However, in this glass system, the molar volume shows the same behavior with the glass density where they both increase with increase of  $\text{Eu}_2\text{O}_3$  concentration. Sidek *et al.* [19] stated that the molar volume is affected by the bond length or inter-atomic spacing between atoms. In this glass system,  $\text{TeO}_2$  is replaced by  $\text{Eu}_2\text{O}_3$  where the bond length of Te-O and Eu-O are  $1.99 \text{ \AA}$  and  $2.04 \text{ \AA}$ , respectively. On the other hand, their respective ionic radius is  $0.52 \text{ \AA}$  and  $0.947 \text{ \AA}$ . The replacement of  $\text{Eu}_2\text{O}_3$  with longer bond length and ionic radius is believed to contribute to the increment of molar volume. This also indicates that the addition of  $\text{Eu}_2\text{O}_3$  may break the structure of the glass by the formation of NBOs. Consequently, the spatial distances in the system increase and loosen the structure [20]. Rada *et al.* suggest that the increase in molar volume is due to the excess oxygen from  $\text{Eu}_2\text{O}_3$  that are not filling the interstices of glass network but they form Eu-O-Eu bond [21].

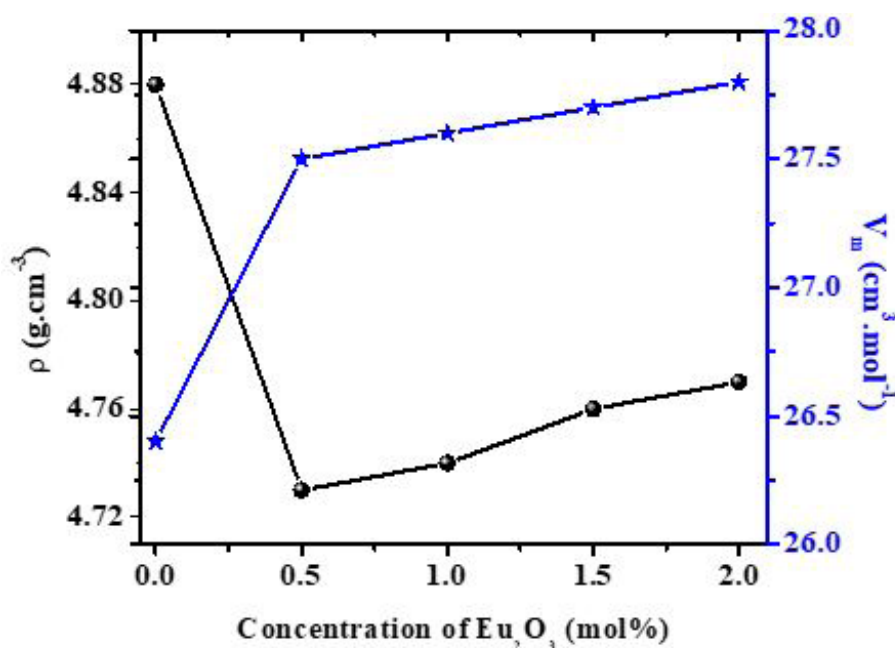


Figure 1: Compositional variation of density and molar volume of TLLEx glasses

Glass Sample	$\rho$	$V_m$	$N_{RE}$	$R_p$	$R_i$
TLLE 0.0	$4.88 \pm 0.01$	$26.4 \pm 0.2$	-	-	-
TLLE 0.5	$4.73 \pm 0.02$	$27.5 \pm 0.1$	1.10	8.42	20.89
TLLE 1.0	$4.74 \pm 0.01$	$27.6 \pm 0.1$	2.18	6.70	16.61
TLLE 1.5	$4.76 \pm 0.03$	$27.7 \pm 0.2$	3.26	5.86	14.54
TLLE 2.0	$4.77 \pm 0.03$	$27.8 \pm 0.2$	4.33	5.33	13.22

**Table 1:** Density,  $\rho$  (g.cm<sup>-3</sup>), ion concentration, NRE ( $\times 10^{20}$  ions.cm<sup>-3</sup>), molar volume,  $V_m$  (cm<sup>3</sup>.mol<sup>-1</sup>), polaron radius,  $R_p$  (Å) and inter-nuclear distance,  $R_i$  (Å) of Eu<sup>3+</sup>-doped lithium tellurite glass

The ion concentration, polaron radius and inter-nuclear distances are also calculated and summarized in Table 1. A direct relation between the increases of ion concentration with increasing Eu<sup>3+</sup> ions is evident. An inverse relation is observed between the ion concentration and inter-nuclear distance. Thus a perfect connected for the current samples could be expected. In contrast, the polaron radius and inter-nuclear distance for Eu-Eu ions shows an expected decrease on increasing Eu<sub>2</sub>O<sub>3</sub> content. This is most likely due to the glass system become packed by rare earth existence hence average rare earth-oxygen distance decrease [22]. However, the value of polaron radius is smaller (8.420 Å – 5.326 Å) than the inter-nuclear distance (20.893 Å – 13.215 Å) which suggesting the formation of small polaron.

### XRD pattern

Figure 2 displays the typical XRD pattern of TLLE 2.0 glass. Complete absence of any sharp peak in the XRD pattern and the appearance of a broad hump in the angular range of 15-35° verified the true amorphous nature of the proposed glass. The occurrence of halo pattern clearly indicated the absence of long-range atomic arrangement or three-dimensional network periodicity in the prepared material.

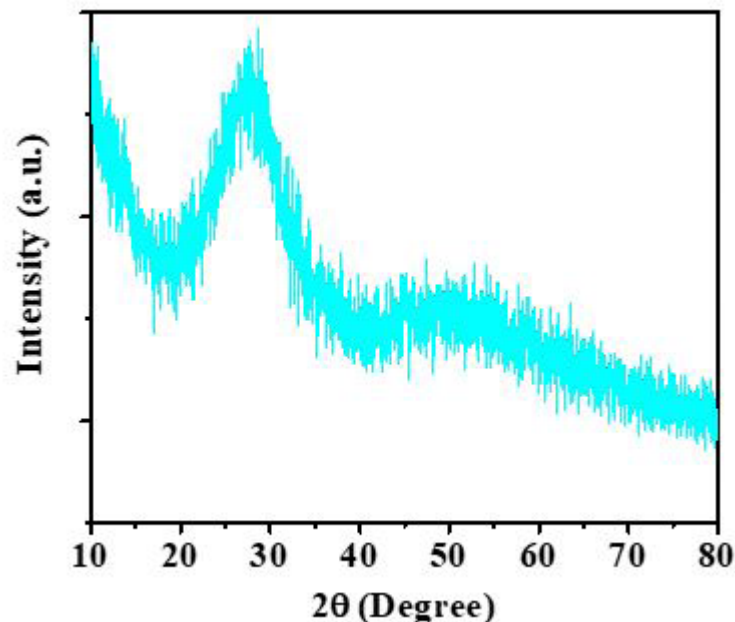


**Figure 2:** Eu<sup>3+</sup> ions concentration (mol%) dependent XRD patterns of TLLE 2.0 glass sample

## Ionic conductivity

### Temperature dependent conductivity

A deeper insight into the electrical properties of the glasses can be obtained from the complex impedance plane plot analysis. The impedance ( $Z''(\omega)$  and  $Z'(\omega)$ ) in the frequency range of 100 Hz–1 MHz of the studied glasses were recorded and found to exhibit non-ideal semicircle (Cole-Cole plots) which could be originated from the dielectric dispersion in the glasses. The typical complex impedance cole-cole plots (Nyquist plots) obtained at a representative temperature, 373 K, for the case of TLLE 0.0 glass is depicted in Figure 3. The cole-cole diagram of the all the investigated glasses exhibited similar behavior with a single semicircle which specified a single relaxation process. Table 2 enlists the estimated values of cole-cole parameters of studied glasses and their codes. The presence of an inclined spike (and arc) on the lower frequency side of the semicircle was resulted from the ionic adsorption and accumulation at the interface with the blocking electrode, as well as charge transfer [23]. Therefore, the conductivity of the glass system was assumed as mainly ionic. This behavior of cole-cole plots was characteristic of the conducting nature of the glass samples. The intercept of the semicircle with real axis on the low frequency side was normally referred as the bulk resistance ( $R_b$ ) of the glass samples. The bulk resistance of the glass can be obtained through circle fit by using ZView Version 2.5b. The intercept of the semicircle was shifted towards the higher  $Z'$  value with the increase of  $\text{Eu}^{3+}$  ions content, indicating the increase in the bulk resistance and thereby decreasing conductivity. From Figure 3, the magnitude of conductivity can be calculated as following:

$$\sigma = \frac{d}{R_b A} \quad (6)$$

where  $d$  is thickness of sample and  $A$  is the area of conductance of sample. The variation of conductivity of these glasses can be well represented by Arrhenius equation.

$$\sigma = \sigma_0 \exp\left(-\frac{E_a}{k_B T}\right) \quad (7)$$

where  $E_a$  is activation energy,  $\sigma_0$  is pre-exponential factor,  $k_B$  is Boltzmann's constant;  $8.617 \times 10^{-5}$  eV  $\text{K}^{-1}$ , and  $T$  is temperature. The variation of the corresponding conductivities for the TLLE $x$  series of glasses is shown in Figure 4 in a semi-log plot as a function of inverse temperature.

The conductivity was found to increase with increase in temperature (see Table 2), which reveals the semiconducting nature of the present glass samples [24]. The charge carrier may be thermally stimulated at higher temperatures. The increasing temperature decreases the electrostatic binding energy which ease the mobility of  $\text{Li}^+$  ions, henceforth the conductivity increase [25]. The electrical conductivity, at all studied frequencies, decreased with increase in the rare earth ion concentration. The electrical conductivity, at all studied frequencies, decreased with increase in the rare earth ion concentration. On the other hand, the activation energy is the amount of electrostatic term which combines the mean barrier height created by the Coulomb forces and the energy of migration [26]. The activation energy ( $E_a$ ) is calculated from the slope fitting lines using Equation (7) and is shown in Figure 5. In Table 3, the values of the activation energy have been presented at different concentration of  $\text{Eu}_2\text{O}_3$ . From Figure 5, it can be seen that the conductivity decrease while the activation energy increase with increase  $\text{Eu}_2\text{O}_3$  concentration. The dependence of conductivity on activation energy suggest that the decrease of conductivity is directly related to the decrease of movement of lithium ions [18]. The decrement in the conductivity can be related to the addition of  $\text{Eu}_2\text{O}_3$  which lead to the increasing of density of the glass network. In addition, the heavy atomic mass of the RE partially prevented the lithium ion movement thus lead to the decrement of conductivity [24, 27]. The activation energy increase from 0.10 eV to 0.23 eV as the concentration of  $\text{Eu}_2\text{O}_3$  increased. It is suggested that the more  $\text{Eu}_2\text{O}_3$  added to the glass network, the glass become more packed. Hence, the vacant sites for  $\text{Li}^+$  mobility decrease. This leads to the reduction of polaronic hopping distance. Therefore, more energy is required for charge carrier transportation [14, 18].

K	10 <sup>3</sup> /T	TLLE 0.0			TLLE 0.5			TLLE 1.0			TLLE 1.5			TLLE 2.0		
		R <sub>b</sub>	σ	Log σ												
298	3.36	5.01	1.33	-6.88	6.08	1.02	-6.99	5.59	1.25	-6.90	6.05	0.98	-7.01	6.27	1.05	-6.98
323	3.10	4.69	1.42	-6.85	6.06	1.03	-6.99	6.20	1.66	-6.78	6.12	0.97	-7.01	5.68	1.16	-6.94
348	2.87	4.26	1.56	-6.81	5.46	1.14	-6.94	5.14	2.01	-6.70	5.39	1.10	-6.96	4.50	1.46	-6.83
373	2.68	4.35	1.53	-6.82	4.63	1.34	-6.87	4.30	2.40	-6.62	5.38	1.10	-6.96	4.46	1.47	-6.83
398	2.51	4.11	1.62	-6.79	4.17	1.49	-6.83	4.00	1.74	-6.76	4.49	1.32	-6.88	4.13	1.59	-6.80

Table 2: Bulk resistance, R<sub>b</sub> (× 10<sup>8</sup> Ω) and conductivity, σ (× 10<sup>-7</sup> S cm<sup>-1</sup>) of the proposed glass samples at constant frequency

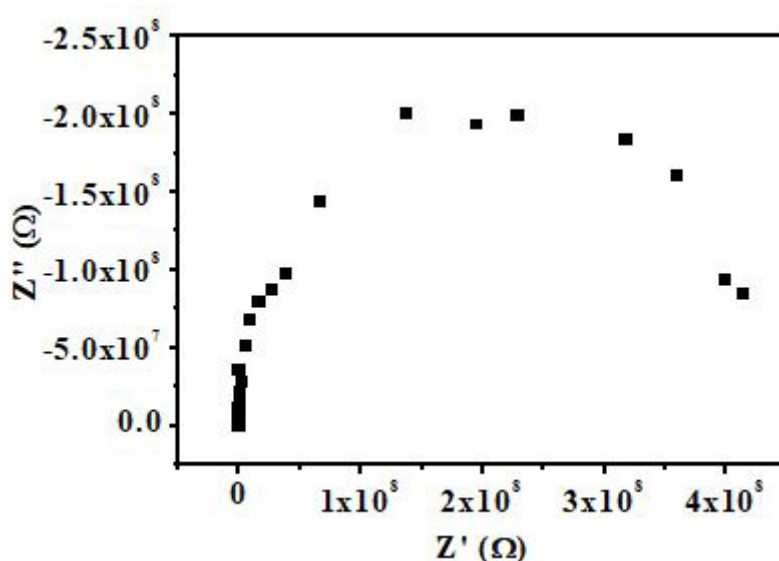


Figure 3: Complex impedance plots of TLLE 0.0 glass at 373 K

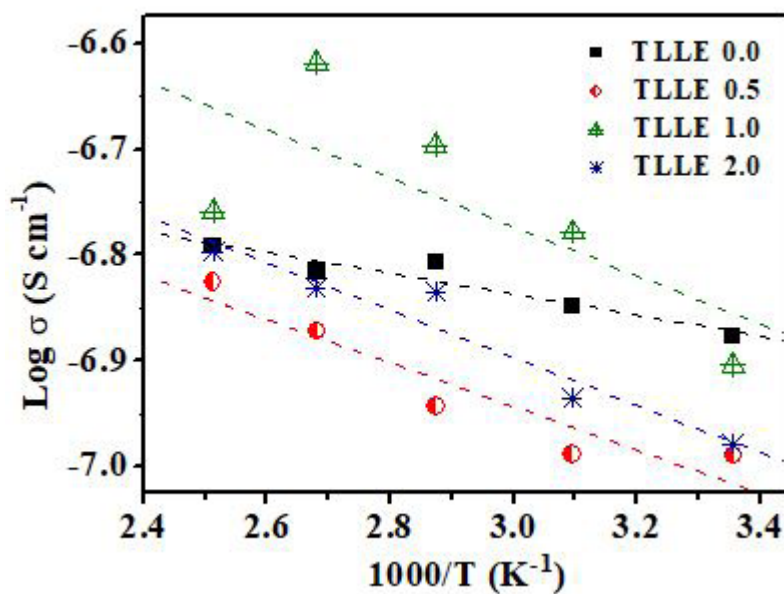
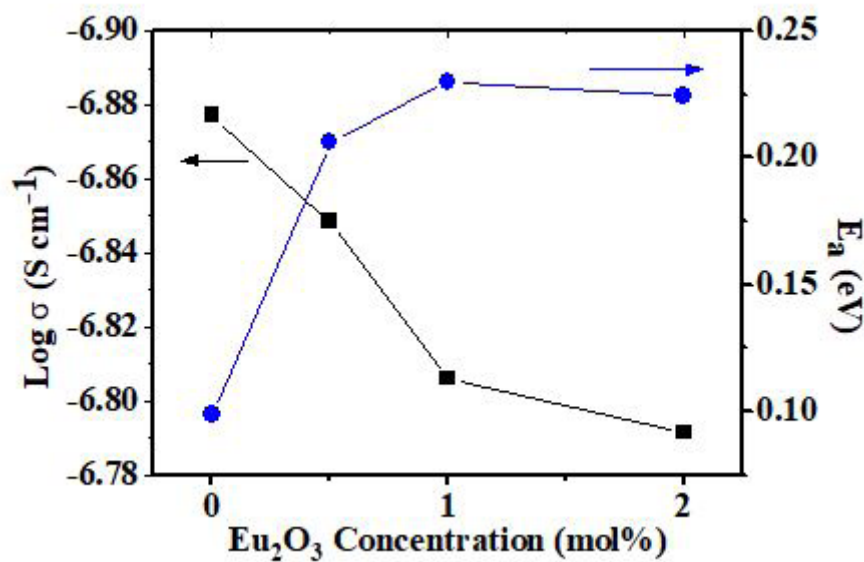


Figure 4: Arrhenius relation of Log(σ) versus 1000/T for all samples

Studied glass	$E_a$	$\epsilon'$	$\tan \delta$	$N(E_f)$
TLLE 0.0	0.10	17.70	0.097	21.3
TLLE 0.5	0.21	13.48	0.087	19.7
TLLE 1.0	0.23	11.52	0.078	23.0
TLLE 1.5	0.23	10.63	0.073	19.8
TLLE 2.0	0.10	9.81	0.055	17.3

**Table 3:** Values of  $E_a$ ,  $\epsilon'$ ,  $\tan \delta$  and  $N(E_f)$  ( $\times 10^{20} \text{ eV}^{-1} \text{ cm}^{-3}$ ) for different compositions of glasses at 398 K and in the relaxation frequency



**Figure 5:** Variation of  $\text{Log}(\sigma)$  and activation energy for TLLEx glasses

### Frequency dependence conductivity

To describe the influence of frequency on the conductivity of a material, Jonscher suggested a suitable formula acknowledged as power-law relation [28] which can be expressed as:

$$\sigma(\omega) = A\omega^s \quad (8)$$

The exponent  $s$  represents the degree of interaction between mobile ions with the lattices around them, while the prefactor exponent  $A$  determines the strength of polarizability and  $\omega$  is the angular frequency. Therefore,  $s$  is defined as:

$$s = \frac{\partial(\log \sigma)}{\partial(\log \omega)} \quad (9)$$

The straight line is obtained by least square fitting of experimental data. Various models have been proposed to ascertain the conduction mechanism on the basis of parameter  $s$ . Among these models, quantum mechanical tunnelling model (QMT), correlated barrier hopping model (CBH), small polaron hopping (SPH) and the overlapping large-polaron (OLP) are the most applicable models.

Frequency dependence of total conductivity for 1.5 mol%  $\text{Eu}_2\text{O}_3$ -doped glass at different temperatures is shown in Figure 6. Similar nature of variation of  $\log(\sigma_{ac})$  with  $\log(\omega)$  has been observed in remaining samples. A flat dc plateau can be observed (Figure 6) at low frequencies. From Figure 6 it can be noticed that the ac conductivity ( $\sigma_{ac}$ ) increases as the frequency increases. The frequency dependence of ac conductivity indicates that conduction is attributed to the increase of the thermally activated small polarons hopping (SPH) [24, 29]. In fact, the polaron comprises the electron plus its surrounding lattice deformation. (polarons can also

be formed from holes in the valence band). If the deformation extends over many lattice sites, the polaron is “large” and the lattice can be treated as a continuum. Charge carriers inducing strongly localized lattice distortions form small polarons [30]. At the high frequency, end the curves overlap indicating the possibility of the presence of space charges. This assumption is reasonable since the space charge effect vanishes at higher temperature and frequency. Also, it is observed that the power law fit is good throughout the frequency range, hence single exponent fit seems to be adequate.

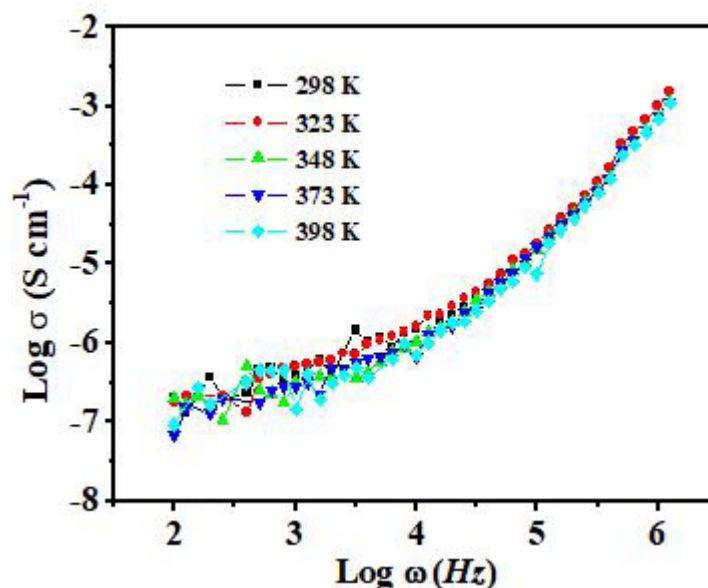


**Figure 6:** Frequency dependence of the conductivity,  $\sigma_{ac}(T)$ , at temperatures shown for the TLLE glass doped 1.5 mol% Eu<sub>2</sub>O<sub>3</sub>

To determine the predominant conduction mechanism of the ac conductivity for the sample, one can suggest the appropriate model for the conduction mechanism in the light of the different theoretical models correlating the conduction mechanism of ac conductivity with  $s(T)$  behavior. If  $s$  is temperature independent, QMT is expected. The CBH is usually associated with a decrease in  $s$  with temperature. SPH conduction is predominant if  $s$  increases with temperature. In the OLP conduction mechanism,  $s$  decreases with temperature reaching a minimum value and then increases again. For the presently studied glass samples, frequency dependence of  $s$  has increasing trends with temperature, suggesting the SPH model (Figure 7). The ac conductivity and frequency exponent expressions of SPH model are given by the following equations:

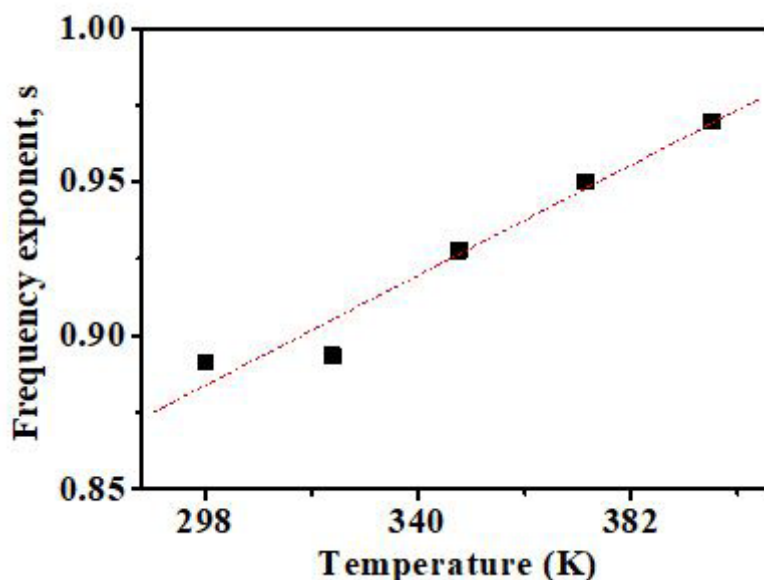


**Figure 7:** Variation of the exponent parameter,  $s$  with temperature for TLLE 2.0 glass

$$s = 1 - \frac{4}{\hbar \left( \frac{1}{\omega_0} \right) - \frac{W_H}{K_B T}} \quad (10)$$

where  $\tau_0$  is the characteristic relaxation time which is of the order of  $\tau_0 = 10^{-13}$  s,  $W_H$  is energy for polaron transfer, and  $T$  is the temperature. Generally, for ionic conductivity, the power law exponents ( $s$ ) may lie between 1 and 0.5, representing ideal long-range pathways and diffusion-limited hopping [55]. In our work,  $s$  is less than unity, the result suggests the polaron conduction.

According to this model, the ac conductivity is given by the following equation

$$\sigma_a = \frac{(\pi e)^2 k_B T \alpha^{-1} \omega [N(E_F)]^2 R_\omega^4}{\rho} \quad (11)$$

Where

$$R_\omega = \frac{1}{2\alpha} \left[ \hbar \left( \frac{1}{\omega_0} \right) - \frac{W_m}{k_B T} \right] \quad (12)$$

where  $\alpha^{-1}$  is the spatial extension of the polaron,  $N(E_F)$  is the density of states near the Fermi level,  $R_\omega$  is the tunneling distance and  $W_m$  is the maximum height of the barrier over which carriers must hop.

Using the equation (11), the density of defect energy state,  $N(E_F)$  at 298 K is obtained and listed in Table 3. From Table 3, a plot of density of defect energy state against  $\text{Eu}_2\text{O}_3$  concentration can be made and is shown in Figure 8. It can be seen that the value of  $N(E_F)$  obtained are found to be around  $\sim 10^{20} \text{ eV}^{-1} \text{ cm}^{-3}$  which suggest that the localized states are near Fermi level [31-33]. The value of  $N(E_F)$  is found to decrease from  $21.3 \times 10^{20} \text{ eV}^{-1} \text{ cm}^{-3}$  to  $17.3 \times 10^{20} \text{ eV}^{-1} \text{ cm}^{-3}$  as the concentration of  $\text{Eu}_2\text{O}_3$  increased. This can be explained by the decreasing disorder in the glass network [34]. The introduction of  $\text{Eu}_2\text{O}_3$  into the glass leads to the creation of quasi-molecular complexes that is the condition where the rare earth coordinated to the non-bridging oxygen which are attached to glass network at one end. The formation of quasi-molecular complexes are believed to have a reasonably constant coordination polyhedron [15]. The lowering value of  $N(E_F)$  also indicate the decreasing presence of charge carrier in the glass network [35].

## Dielectric Investigation

Dielectric relaxation studies are important to understand the nature and the origin of dielectric losses, which may be useful in determining the structure and defects in solids. The dielectric relaxation is described by a Cole-Cole model. Dielectric properties of glasses are complex functions of frequency, shape, dimension, and spatial ordering of the constituent atoms. The real ( $\epsilon'$ ) and imaginary ( $\epsilon''$ ) parts of dielectric constant were calculated via:

$$\epsilon' = \frac{C}{\epsilon_0 A} \quad (13)$$

and

$$\tan \delta = \frac{\epsilon''}{\epsilon'} \quad (14)$$

where  $C$  is the capacitance of the sample,  $\epsilon_0$  is the permittivity of free space ( $8.8542 \times 10^{-12} \text{ F/m}$ ),  $A$  is the cross-sectional area of the electrode and  $\tan \delta$  is the dissipation factor or loss tangent. The frequency dependence of the dielectric constant ( $\epsilon'$ ) and loss factor ( $\tan \delta$ ) are studied for the TLLE 1.5 glass sample and shown in Figure 9(a) and (b). The temperature dependence of  $\epsilon'$  and  $\tan \delta$  (case of TLLE 1.5 glass sample) as a function of logarithmic frequency at several temperatures is depicted in Inset of Figure 9(a) and (b). It is observed that dielectric constant measured at lower frequency is greater than higher frequency at all temperature. The larger values of dielectric constant at low frequencies is attributed to the role of more charge carriers at the interfaces, which can contribute in increasing net dipoles on interface. These dipoles alter the net polarization of the ionic medium, which contributes

to dielectric constant. Whereas at higher frequencies, the periodic reversal of the applied field takes place so quickly such a way that there is less time for polarization to form completely and no charge buildup at the interface resulting in constant  $\epsilon'$  value. Atomic and electronic polarization usually occurs at higher frequency. In accumulation, as shown in the insert of Figure 9, that the value of dielectric constant show considerable increase with temperature and the increment is more pronounced at frequencies lower than 100 Hz. The increasing dielectric constant with temperature can be explained by the weakening of bond energy. Hence, the intermolecular forces decreases which results in the increase of orientational vibration [12, 36]. The charge carrier acquired thermal energy hence they are able to move freely within the glass network [37].

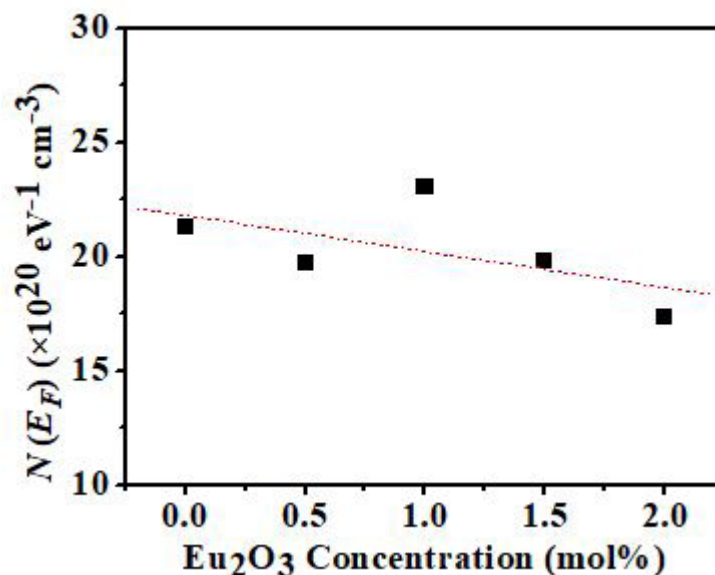


Figure 8: The calculated density of localized state,  $N(E_F)$  as function of  $\text{Eu}_2\text{O}_3$  concentration at 298 K

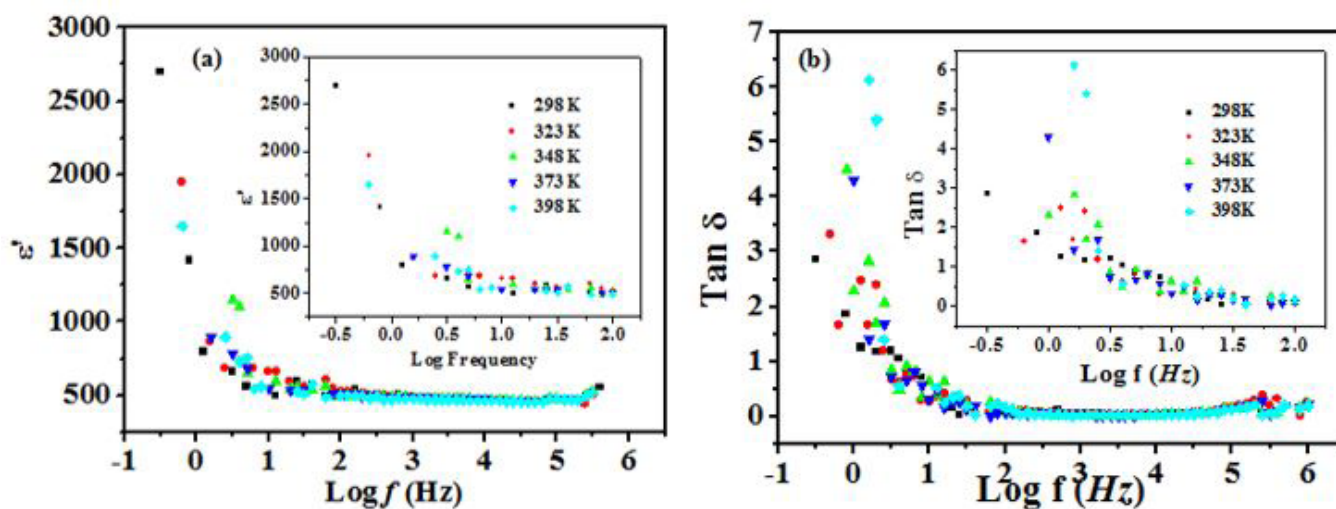


Figure 9: The frequency dependence curves at room temperature of dielectric constant  $\epsilon'(\omega)$  (a) and loss factor (b) for TLLE1.5 glass sample. Inset shows the variation of  $\epsilon'(\omega)$  and  $\tan(\delta)$  at different temperatures case of 1.5 mol%  $\text{Eu}_2\text{O}_3$

The dielectric constant,  $\epsilon'$  and Dissipation factor ( $\tan \delta$ ) are tabulated in Table 3. The dielectric constant is observed to decrease from 17.70 to 9.81 with  $\text{Eu}_2\text{O}_3$  concentration. Such behavior is similar to that exhibit by ac conductivity. The large molecular mass of  $\text{Eu}_2\text{O}_3$  acts as hindrance to the mobility of charge carrier, hence there is decrease of electronic polarization contribution to the total polarizability [12, 24]. The electronic polarization is part of the total polarization where it is a polarization that occur due to the displacement of valence electron relative to the positive nucleus [38].

Dissipation factor ( $\tan \delta$ ) measures the inefficiency of the insulator. When an insulator is applied to an electric field, the heat is emitted due to the high resistance of the insulator. From Figure 9(b), the increasing value of dissipation factor with increasing temperature is more pronounced at frequency below 100Hz. However, it starts to decrease at higher frequency and remain almost

constant. The dissipation factor dependence of frequency is associated with losses by conduction or mobility of charge carriers inside the glass network in addition to the electron polarization loss [39]. The high value of dissipation factor at low frequency suggests that charge carriers are able to move around hence promoting dielectric loss. As the frequency increase, the mobility of charge carriers decrease hence ion vibration is the only source of dielectric loss [24].

From Table 3, it is observed that the dissipation factor decrease from 0.097 to 0.055 with increasing  $\text{Eu}_2\text{O}_3$ . This is due to the heavy mass of  $\text{Eu}_2\text{O}_3$  ( $351.93 \text{ g mol}^{-1}$ ) that acts as hindrance to the movement of charge carrier. The suppressed movement of charge carrier leads to the decreasing conductivity and dielectric loss. With  $\text{Eu}^{3+}$  acts as hindrance to the movement of  $\text{Li}^+$  ion, there is decrement of electronic contribution to the total polarizability [12, 24].

## Optical properties

### Absorption spectra

The room temperature UV-Vis-NIR absorption spectra recorded in the range of 350–700 nm of selected glass samples are presented in Fig. 10. The absorption bands located at 464 and 533 nm were ascribed to the electronic transitions from  ${}^7\text{F}_0 \rightarrow {}^5\text{D}_2$  and  ${}^7\text{F}_1 \rightarrow {}^5\text{D}_1$  of  $\text{Eu}^{3+}$  ions, respectively. Overall, the spectral profile of every sample was altered accompanied by a slight peak shift for each band. These alterations in the absorption peak positions were attributed to the Stark splitting of the degenerate  $4f$  levels in the presence of the host material's crystalline field. This observation clearly indicated the homogeneous incorporation of  $\text{Eu}^{3+}$  ions (without agglomeration) into the tellurite glass network. Moreover, the slight peak shift was ascribed to the variation of ligand field strength at the REIs site. Generally, the  $4f$  inner shell behaviour of REIs is not affected by the surrounding  $\text{Eu}^{3+}$  ions that produce effective shielding on  $4f$  electrons by the completely filled  $5s$  and  $5p$  shells. This creates more intense lower energy bands compared to the higher one [40].

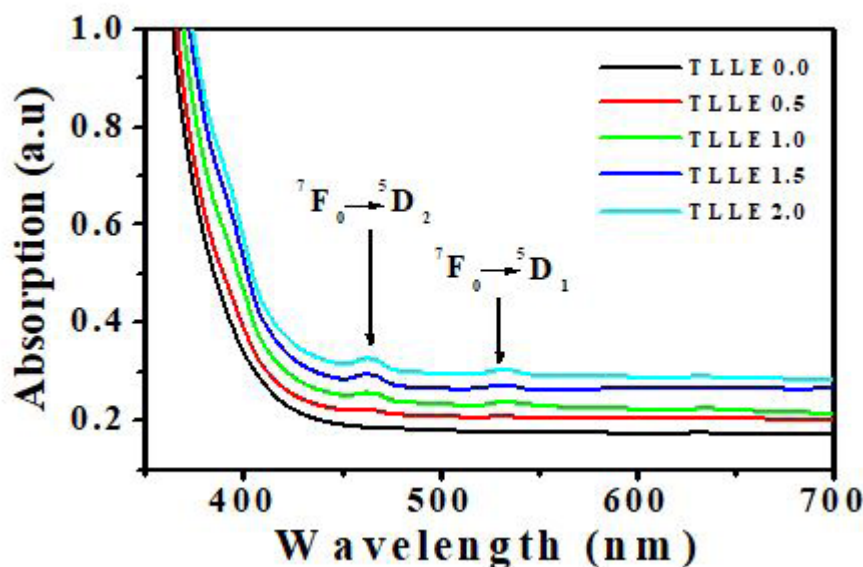


Figure 10: Absorption spectra of glass samples in the UV-Vis region

The Davis and Mott theory [41] was used to evaluate the direct and indirect optical band gap energy of the amorphous materials. In both the transitions, the electromagnetic waves interact with the electrons in the valence band across the fundamental gap and rise to the conduction band [42, 43]. According to Davis and Mott, the absorption coefficient  $\alpha(\nu)$  can be expressed as a function of photon energy ( $h\nu$ ) for the direct and indirect allowed transition:

$$\alpha(\nu) = B \frac{(h\nu - E_g)^r}{h\nu} \quad (15)$$

where  $r$  is the index number. In Figure 11 (a) and (b), the Tauc's plots of the TLLE $x$  glass sample are drawn between  $(\alpha h\nu)^{1/n}$  and photon energy ( $h\nu$ ), by substituting the value  $r = 1/2$  in Eq. (15) for direct allowed transitions and  $r = 2$  for indirect allowed transitions. Here,  $B$  is constant,  $E_g$  is the optical band gap and  $\alpha(\nu)$  is the absorption coefficient represented by:

$$\alpha(\nu) = \frac{2.303A}{t} \quad (16)$$

where  $t$  is the thickness of the sample and  $A$  corresponds to absorbance. The optical band gap values were obtained from the linear part of the curves extrapolating at  $(\alpha h\nu)^2 = 0$  and  $(\alpha h\nu)^{1/2} = 0$  for direct and indirect transitions, respectively. The absorption coefficient  $\alpha(\nu)$  near the absorption band edge exhibit an exponential behavior on the photon energy ( $h\nu$ ) and obeys the empirical relation given by Urbach [44].

$$\alpha(\nu) = \alpha_0 \exp(h\nu/\Delta E) \quad (17)$$

where  $\alpha_0$  is a constant and  $\Delta E$  is the Urbach energy which is calculated by the inverse slope of the  $\ln \alpha$  against  $h\nu$  in the lower photon energy level. This exponential behavior is due to the band tails associated with the valence and conduction bands which extends into the band gap.

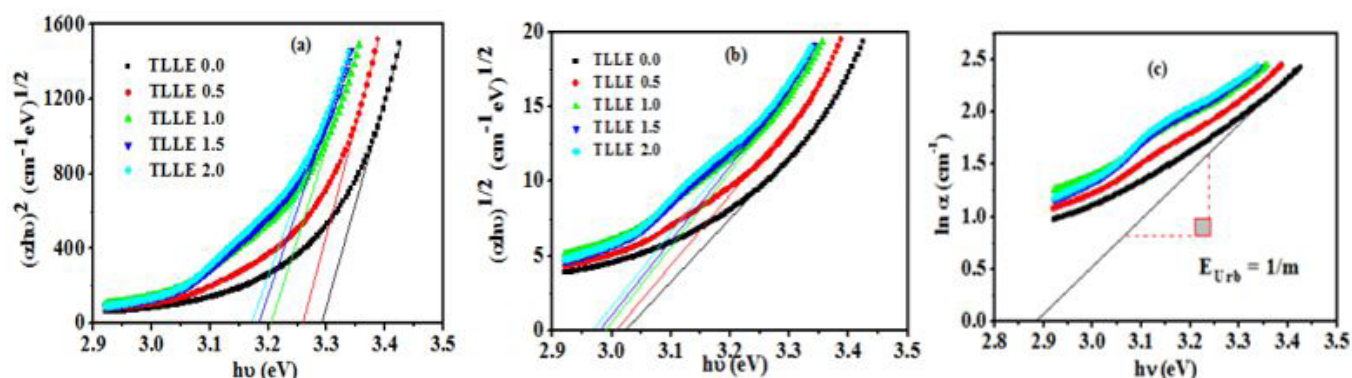


**Figure 11:** The values of band gap energy for (a) indirect, (b) direct allowed transitions and the (c) Urbach energy for the prepared glass sample

The values of band gaps and Urbach energy of the prepared samples are listed in Table 4. The results in Table 4 depicts that the direct and indirect optical band gaps decrease from 3.29 and 3.07 eV to 3.17 and 2.97 eV, respectively, as the concentration of  $\text{Eu}^{3+}$  ions is increased up to 2 mol%. The decreasing value of optical band gap energy by increasing the  $\text{Eu}_2\text{O}_3$  content can be understood in terms of the structural change that are taking place. It is generally accepted that the location of absorption edge depends on the oxygen bond strength in the glass forming network [45]. The introduction of RE changes the oxygen bonding in glass forming network and any change of oxygen bonding in glass network such as the formation of non-bridging oxygen (NBO) changed the absorption characteristics. Conversely, when one molecule of  $\text{Eu}_2\text{O}_3$  was introduced into the tellurite matrix, coordination number of Te atoms was changed. Optical band gap was influenced not only by the chemical composition but also by a structural arrangement of the host matrix. It has been shown from ab initio molecular orbital calculations that the difference between Homo- and Lumo-state is low for  $\text{TeO}_4$  unit whereas it is high for  $\text{TeO}_3$  [46] and even for  $\text{TeO}_{3+1}$  units [47]. It signified that broader optical band gap can be observed for  $\text{TeO}_2$  based glasses if the density of  $\text{TeO}_3$  and/or  $\text{TeO}_{3+1}$  unit assisted significantly to the network formation. However, these changes were not sufficient to account for the observed decrease in the optical band gap. With the substitution of Li into  $\text{TeO}_2$ , bridging Te–O–Te bonds are broken and non-bridging Te–O– $\text{Li}^{2+}$  bonds were formed. The NBO bonds have a much greater ionic character and much lower bond energies. Consequently, the NBO bonds have higher polarizability and cation refractions [46, 47].

Glass Sample	$E_{ind}$	$E_{dir}$	$\Delta E$
TLLE 0.0	$3.07 \pm 0.01$	$3.29 \pm 0.01$	$0.226 \pm 0.001$
TLLE 0.5	$3.01 \pm 0.01$	$3.26 \pm 0.01$	$0.230 \pm 0.002$
TLLE 1.0	$2.99 \pm 0.01$	$3.20 \pm 0.01$	$0.280 \pm 0.002$
TLLE 1.5	$2.98 \pm 0.01$	$3.19 \pm 0.01$	$0.290 \pm 0.002$
TLLE 2.0	$2.97 \pm 0.01$	$3.17 \pm 0.01$	$0.308 \pm 0.001$

**Table 4:** Direct,  $E_{dir}$  (eV), and indirect,  $E_{ind}$  (eV) band gaps and Urbach energy,  $\Delta E$  (eV) of the proposed TLLEx glasses

The existence of  $\Delta E$ , or band tail in the forbidden energy band gap in glass and amorphous materials represented the disorder in the material [20]. The value of Urbach energy of TLLE $x$  glass sample is shown in Figure 11(c). In Table 4, the  $\Delta E$  values of the synthesised glasses were found to be increased from 0.226 to 0.308 eV with the addition of  $\text{Eu}^{3+}$  content. It was evident that by increasing the concentration of  $\text{Eu}^{3+}$  ions in present glass system, Urbach energy values were increased due to the increased disorder in the glass.

### Photoluminescence spectra

The room temperature PL spectrum for samples without and with  $\text{Eu}_2\text{O}_3$  is shown in Figure 12(a), in the range of 500-750 nm upon 393 nm excitation. The relative luminescence intensity peak of such glasses is shown in Figure 12(b). Six evidenced emission bands centered at 532 (green), 552 (deep-green), 586 (orange), 613 (red), 649 (deep-red) and 697 nm (deep-red) nm were assigned to the transitions of  $^5\text{D}_1 \rightarrow ^7\text{F}_1$ ,  $^5\text{D}_0 \rightarrow ^7\text{F}_0$ ,  $^5\text{D}_0 \rightarrow ^7\text{F}_1$ ,  $^5\text{D}_0 \rightarrow ^7\text{F}_2$ ,  $^5\text{D}_0 \rightarrow ^7\text{F}_3$  and  $^5\text{D}_0 \rightarrow ^7\text{F}_4$  of  $\text{Eu}^{3+}$  ion, respectively. An increase in the efficient emission was observed (Fig. 12(b)) with the increase of  $\text{Eu}_2\text{O}_3$  content up to 2.0 mol%. As the concentration of RE species was increased up to a certain value the optical gain showed an increasing trend.

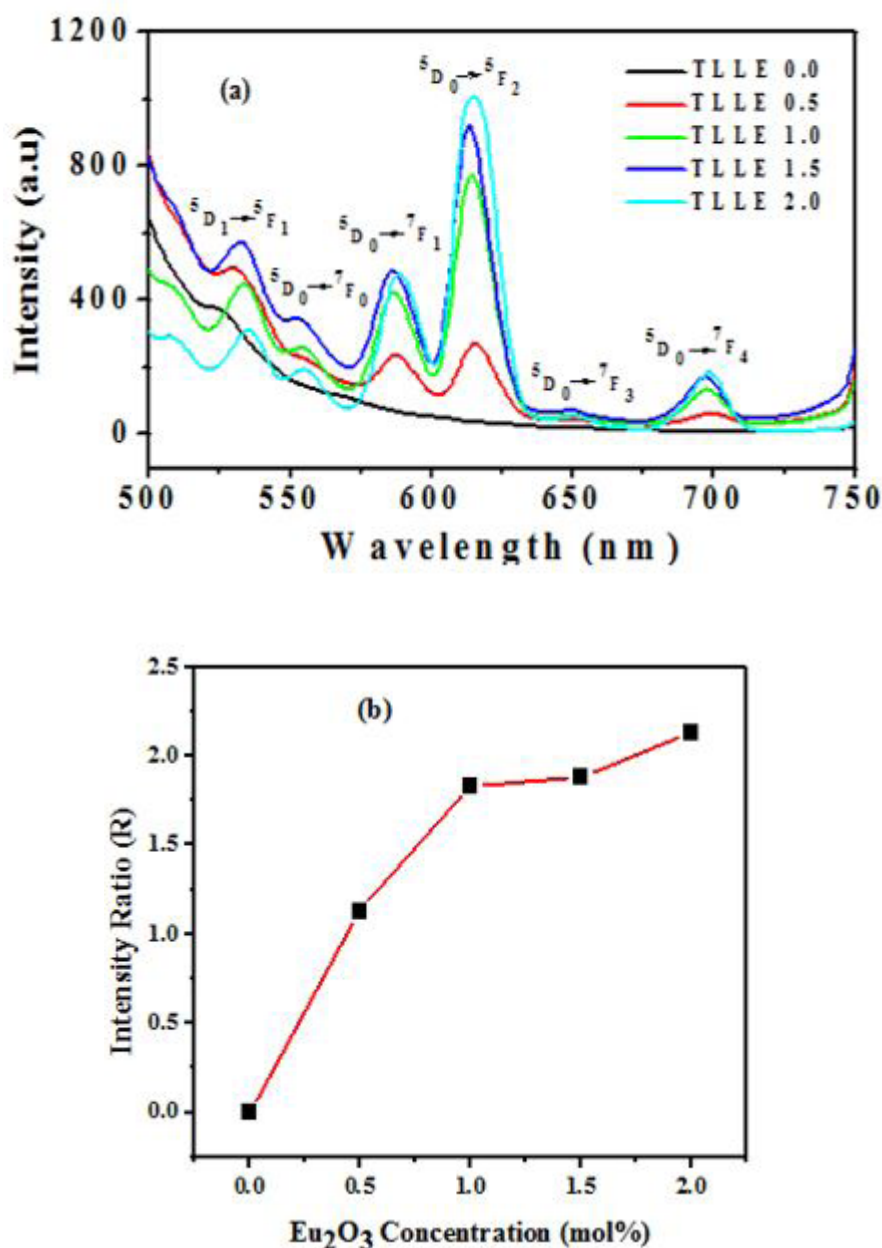


Figure 12(a): Photoluminescence spectra of the prepared glasses and (b) intensity ratio against  $\text{Eu}_2\text{O}_3$  concentration

Sharp peak with highest intensity is observed at transition  ${}^5D_0 \rightarrow {}^7F_2$  (613 nm) which is in red region. The  ${}^5D_0 \rightarrow {}^7F_1$  ( $J = 2$  and 4) transitions are electric dipole (ED) transitions while another transition  ${}^5D_0 \rightarrow {}^7F_1$  (586 nm) could be found as magnetic dipole transition [48, 49]. Electric dipole transition has greater probability than the magnetic dipole transition when  $\text{Eu}^{3+}$  ions are located at low symmetry environment [50]. On the other hand, the presence of transition  ${}^5D_0 \rightarrow {}^7F_0$  (552 nm) indicated the low symmetry environment of lithium tellurite glass upon the presence of  $\text{Eu}^{3+}$  ion [51]. This can be confirmed by the intensity ratio which has the formula as following:

$$R = \frac{I({}^5D_0 \rightarrow {}^7F_2)}{I({}^5D_0 \rightarrow {}^7F_1)} \quad (18)$$

The intensity ratio,  $R$  indicates the symmetry around  $\text{Eu}^{3+}$  ions where a higher value of  $R$  shows that the symmetry around  $\text{Eu}^{3+}$  is lower [52]. The calculated  $R$  for all sample are shown in Figure 12. A higher value of  $R$  shows a better quality of host matrix for laser application [53]. The  $R$  values of the presented lithium tellurite glasses are found to be 1.13, 1.83, 1.88 and 2.13 for TLLE 0.5, TLLE 1.0, TLLE 1.5 and TLLE 2.0 glasses respectively. With considerably high  $R$  values of glass sample, TLLE 2.0 is suggested for potential laser applications. The region around  $\text{Eu}^{3+}$  becomes more asymmetry with increment of  $\text{Eu}_2\text{O}_3$  addition [52]. The  $\text{Eu}^{3+}$  ions break the Te-O-Te linkage and create non-bridging oxygen around the structure. Therefore, the structure around the dopant becomes random and irregular. The intensity ratio of the prepared glasses is comparatively on the higher side than the other reported  $\text{Eu}^{3+}$  doped oxide glass.

The possible energy level of  $\text{Eu}^{3+}$  in lithium tellurite glass is shown in Figure 13. From Figure 13, upon the excitation at 393 nm, the  $\text{Eu}^{3+}$  ions are excited from  ${}^7F_0$  to  ${}^5L_6$  level by ground state absorption. Nonradioactive decay through multiphoton relaxation takes place which results in the population of  ${}^5D_0$  and  ${}^5D_1$  level. As the result, transition  ${}^5D_1 \rightarrow {}^7F_1$  and  ${}^5D_0 \rightarrow {}^7F_1$  ( $J = 0, 1, 2, 3, 4$ ) can be observed throughout the spectra. This is in agreement with other researcher [52, 54, 55].

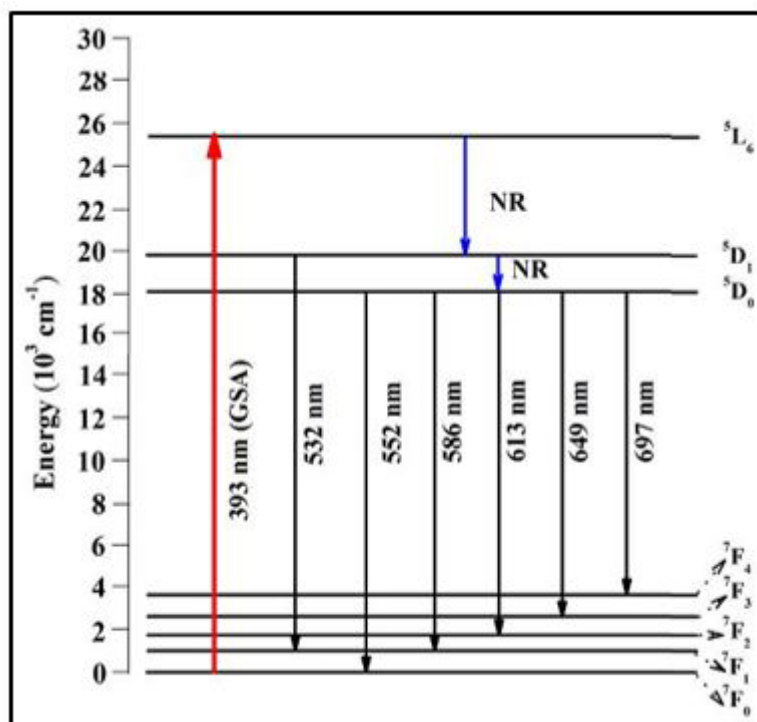


**Figure 13:** Energy level diagram of the prepared glass system (GSA and NR signify ground state absorption and nonradiative processes respectively)

## Conclusion

We examined the physical, optical and dielectric properties of  $\text{Eu}_2\text{O}_3$  doped lithium tellurite glasses synthesized via melt quenching method. Glasses were characterized using various analytical tools. The influence of  $\text{Eu}^{3+}$  dopant concentration on conductivity, dielectric constant and loss tangent are determined using Impedance Analyzer. The temperature dependence conductivity is found

to follow the Arrhenius equation. The conductivity decrease while activation energy,  $E_a$  increase with  $\text{Eu}_2\text{O}_3$  concentration. The frequency dependent conductivity is found to follow the power law. The density of states is calculated using SPH model and found to be decrease with  $\text{Eu}_2\text{O}_3$  concentration. The dielectric constant and loss tangent decrease with both frequency and  $\text{Eu}_2\text{O}_3$  concentration. The optical band gap energy value for the direct and indirect allowed transitions were occurred in the range of 3.29 and 3.07 eV to 3.17 and 2.97 eV, respectively. The PL spectra revealed six prominent peaks with gradual increase in the peak intensity as a function of  $\text{Eu}^{3+}$  ions doping. Our study may provide useful information towards the device fabrication using  $\text{Eu}^{3+}$ -doped lithium tellurite glass.

## Acknowledgements

The authors would like to express their gratitude to the Government of Malaysia through grant vote 03E78 for the financial support of this project. Thanks are also due to UTM through RMC for awarding the Postdoctoral fellowship to the first author.

## References

1. M Rajesh, GR Reddy, NJ Sushma, G Devarajulu, BDP Raju (2020) *Optic. Mater.* 107: 110038.
2. G Lakshminarayana, KM Kaky, SO Baki, A Lira, P Nayar, et al. (2017) *J. Alloys. Compd.* 690: 799.
3. N Elkhoshkhany, Eslam Syala, El Sayed Yousef (2019) *Results Phys* 14: 102370.
4. K Tanaka, Y Toshinobu, H Yamada, K Kamiya (1988) *J Alloys. Compd* 103: 250.
5. Y Iwadate, H Kenmotsu, T Hattori (2000) *J. Alloys. Compd.* 305: 130.
6. MM Umair, AK Yahya (2015) *Chalcogenide Letters.* 12: 287.
7. S. Azianty, AK Yahya, MK Halimah (2012) *Mater Chem Phys.* 142: 549.
8. MR Tripathy, R Joshi, NC Mehra, Sanjeev Kumar, RP Tandon (2007) *Mater. Lett.* 61: 585.
9. S Chakraborty H Satou, H Sakata (1997) *J Appl. Phys.* 82: 5520.
10. AA Ali, MH Shaaban (2010) *Solid State Sci.* 12 (2010): 2148.
11. M Abdel-Baki, AM Salem, FA Abdel-Wahab, F El-Diasty (2008) *J Non-Cryst. Solids.* 354: 4527.
12. DD Ramteke, RS Gedam (2014) *Solid State Ionics* 258: 82.
13. AL Moura, LJQ Maia, V Jerez, ASL Gomes, CB de Araújo, et al. (2019) 214: 116543.
14. M Kaky Kawa, G Lakshminarayana, S Baki, I Kityk, Y Taufiq-Yap, et al. (2017) *Results Phys.* 7: 166.
15. MH Shaaban, AA Ali, LK El-Nimr (2006) *J. Mater. Chem. Phys.* 96: 423.
16. M Haouari, FB Slimen, A Maaoui, N Gaumer (2018) *J. Alloy. Compd.* 743: 586.
17. M Ribes, JR Akridge, M Balkanski (1990) *Solid State Microbatteries*, New York.
18. RS Gedam, DD Ramteke (2013) *J. Phys. Chem. Solids.* 74: 1399.
19. HAA Sidek, S Rosmawati, ZA Talib, MK Halimah, WM Daud (2009) *Am. J. App. Sci.* 6: 1489.
20. G Upender, S Ramesh, M Prasad, VG Sathe, VC Mouli (2010) *J. Alloy. Compd.* 504: 468.
21. S Rada, A Dehelean, E Culea (2011) *J. Non-Cryst. Solids.* 357: 3070.
22. RS Gedam, DD Ramteke (2012) *J. Rare Earth.* 30: 785.
23. I Jlassi, N Sdiri, H Elhouichet, M Ferid (2015) *J. Alloy. Compd.* 645: 125.
24. MP Kumar, T Sankarappa, S Kumar (2008) *J Alloy. Compd.* 464: 393.

25. PR Rao, L Pavić, A Moguš-Milanković, VR Kumar, IV Kityk, et al. (2012) *J. Non-Cryst. Solids*. 358: 3255.
26. G Gruener, DDS Meneses, P Odier, JP Loup (2001) *J. Non-Cryst. Solids*. 281: 117.
27. RS Gedam, DD Ramteke (2013) *J. Phys. Chem. Solids*. 74: 1039.
28. AK Jonscher (1996) *Universal Relaxation Law*, Chelsea Dielectrics Press, London.
29. S Hraiech, M Ferid (2013) *J. Alloy. Compd.* 577: 543.
30. YB Saddeek (2009) *J. Alloy. Compd.* 467: 14.
31. PS Rao, C Rajyasree, AR Babu, PMV Teja, DK Rao (2011) *J. Non-Cryst. Solids*. 357: 3585.
32. PS Rao, PR Babu, R Vijay, T Narendrudu, N Veeraiah, et al. (2014) *Mater. Res. Bull.* 57: 58.
33. K Srilatha, KS Rao, Y Gandhi, V Ravikumar, N Veeraiah (2010) *J. Alloy. Compd.* 507: 391.
34. MS Reddy, NG Raju, G Nagarjuna, N Veeraiah (2007) *J. Alloy. Compd.* 438: 41.
35. M Nagarjuna, P Raghava Rao, Y Gandhi, V Ravikumar, N Veeraiah (2010) *Physica B*. 405: 668.
36. DD Ramteke, RS Gedam (2014) *Spectrochimica acta. Part A*. 133: 19.
37. RM Mahani, SY Marzouk (2013) *J. Alloy. Compd.* 579: 394.
38. NA Hegab, HM El-mallah (2009) *Acta Phys. Pol A* 116: 1048.
39. SM Salem, EK Abdel-Khalek, EA Mohamed, MA Farouk (2012) *J. Alloy. Compd.* 513: 35.
40. Sd. ZA Ahamed, CM Reddy, BDP Raju (2013) *J. Spectrochim. Acta A*. 103: 246.
41. EA Davis, NF Mott (1970) *Philos. Mag.* 22: 903.
42. RP Sreekanth Chakradhar, KP Ramesh, JL Raob, J Ramakrishna (2003) *J. Phys. Chem. Solids* 64 (2003) 641.
43. E Wu, H Chen, Zh Sun, H Zeng (2003) *J. Opt. Lett.* 28: 1692.
44. F Urbach (1953) *Phys. Rev.* 92: 1324.
45. BD Mcswain, NF Borrel, SV Gongjen (1963) *J. Phys. Chem. Glasses*. 4: 1.
46. S Akamine, T Nanba, Y Miura, S Sakida (2005) In: 9th biennial worldwide congress on refractories 8.
47. A Berthereau, E Fargin, A Villezusanne, R Olazcuaga, G Le Flem, et al. (1996) *J. Solid. State. Chem.* 126: 142.
48. BDP Raju, CM Reddy (2012) *Optic. Mater.* 34: 1251.
49. CR Kesavulu, KK Kumar, N Vijaya, KS Lim (2013) *Mater. Chem. Phys.* 141: 903.

50. T Som, B Karmakar (2010) *J. Phys.: Condens. Matter.* 22: 035603.
51. TS Barros, BS Barros, S Alves, RHG Kiminami, HL Lira, et al. (2008) *Mater. Sci. Forum.* 591: 745.
52. W Stambouli, H Elhouichet, B Gelloz, M Férid, *J Lumin* (2013) 138: 201.
53. K Maheshvaran, K Marimuthu (2012) *K Maheshvaran, K Marimuthu, J Lumin* (2012) 132: 2259.
54. P Krishnapuram, SK Jakka, C Thummala, RM Lalapeta (2012) *J. Mol. Struct.* 1028: 170.
55. Y Gandhi, IV Kityk, MG Brik, PR Rao, N Veeraiah (2010) *J. Alloy. Compd.* 508: 278.